Journal of Applied Physics

A proof of concept of the bulk photovoltaic effect in non-uniformly strained silicon

Cite as: J. Appl. Phys. **131**, 125706 (2022); https://doi.org/10.1063/5.0074426
Submitted: 08 October 2021 • Accepted: 10 March 2022 • Published Online: 24 March 2022

C. L. Manganelli, S. Kayser and M. Virgilio

View Online Export Citation CrossMark

ARTICLES YOU MAY BE INTERESTED IN

Electron- and proton irradiation of strongly doped silicon of p-type: Formation and annealing of boron-related defects
Journal of Applied Physics **131**, 125705 (2022); https://doi.org/10.1063/5.0078043

Transport properties of a thin GaN channel formed in an $Al_{0.9}Ga_{0.1}N$/GaN heterostructure grown on AlN/sapphire template
Journal of Applied Physics **131**, 124501 (2022); https://doi.org/10.1063/5.0077107

Annealing-temperature-dependent evolution of hydrogen-related donor and its strong correlation with X-photoluminescence center in proton-irradiated silicon
Journal of Applied Physics **131**, 125702 (2022); https://doi.org/10.1063/5.0083249

Lock-in Amplifiers up to 600 MHz
Zurich Instruments
Watch



AIP Publishing

© 2022 Author(s).

Journal of Applied Physics ARTICLE scitation.org/journal/jap

A proof of concept of the bulk photovoltaic effect in non-uniformly strained silicon

Cite as: J. Appl. Phys. **131**, 125706 (2022); doi: 10.1063/5.0074426
Submitted: 8 October 2021 · Accepted: 10 March 2022 ·
Published Online: 24 March 2022

View Online Export Citation CrossMark

C. L. Manganelli,[1,a)] S. Kayser,[2,3] and M. Virgilio[4]

AFFILIATIONS

[1]IHP-Leibniz-Institut für Innovative Mikroelektronik, Im Technologiepark 25, 15236 Frankfurt (Oder), Germany
[2]Weierstrass Institute for Applied Analysis and Stochastics, Mohrenstr. 39, D-10117 Berlin, Germany
[3]IKZ-Leibniz-Institut für Kristallzüchtung, Max-Born-Str. 2, D-12489 Berlin, Germany
[4]Dipartimento di Fisica "Enrico Fermi," Università di Pisa, Largo Bruno Pontecorvo 3, 56127 Pisa, Italy

[a)]**Author to whom correspondence should be addressed:** manganelli@ihp-microelectronics.com

ABSTRACT

We numerically investigate non-uniformly strained Si-based systems to demonstrate that when a well focused laser beam locally excites the sample, the lattice distortion, impacting the band edge profile, causes a spatially dependent photovoltaic effect. It follows that, scanning the sample surface with the pump spot, a photovoltage signal can be acquired and used to quantitatively map the non-uniform strain field. To provide numerical evidence in this direction, we combine mechanical simulations with deformation potential theory to estimate the band edge energy landscape of a Si lattice strained by an array of SiN stripes fabricated on the top surface. These data are then used to simulate the voltage signal obtained scanning the sample surface with a normal incident pump beam. Our analysis suggests that strain deformations as small as 0.1% can trigger at room temperature robust photovoltaic signals. These results allow us to envision the development of a fast, cost-effective, and non-destructive setup, which leverages on the bulk-photovoltaic effect to image the lattice deformation in semiconductor crystals.

Published under an exclusive license by AIP Publishing. https://doi.org/10.1063/5.0074426

INTRODUCTION

In the last two decades, the strain engineering in microstructures has emerged as a powerful tool to modify and optimize electronic and optical properties of semiconductor devices.[1] To mention just a few examples, controlled strain fields have been used to enhance the optical emission rate of Ge or GeSn based devices,[2–7] to improve the electron and hole mobility in Si-based FET,[8] or to induce second order non-linearities in Si photonic structures.[9–12]

As a matter of fact, due to the central role of silicon in the microelectronic industry, several efforts have been devoted to the description of strain-induced modification of its band structure[13] and to the optimization of strained silicon films[14] or nanowires[15] based on this semiconductor material.

The measurement of strain fields in bulk semiconductors or multi-layer structures is routinely achieved by means of x-ray diffraction experiments.[16–18] As an alternative, when the lattice deformation is close to the sample surface, Raman spectroscopy can also be employed. In this case, the strain is measured, evaluating its impact on the energy of the Raman active phonon modes.[19,20] In a μ-Raman setup, where the pump spot size is focused at about 1 μm, it is possible to image spatially non-homogeneous strain fields.[21–23] More recently, spatially resolved maps of the lattice deformation have been obtained leveraging on the strain-induced birifrangence phenomenon, and tools based on this physical effect, as the Scanning Infrared Stress Explorer (SIREX),[24] are already commercially available. In addition, the cross-sectional strain map of semiconductor devices has also been obtained by means of precession electron diffraction devices (PEDs).[25]

X-ray diffraction experiments, Raman setup, SIREX, and PED require quite bulky and costly setup correlated with the high cost of filters, gratings, spectrometers, and optical instrumentation. In addition, most of them may present high sample preparation effort or strong limitations in terms of vertical resolution. As an example, Raman spectroscopy is able to offer a vertical resolution that depends on the laser wavelength but that can be difficult to overcome the limit of 1 μm.

Published under an exclusive license by AIP Publishing

For these reasons and also in view of the increasing importance of the strain engineering in the field of semiconductor devices, novel techniques to measure the lattice strain, able to overcome some of the above-mentioned drawback, are highly desirable.

Here, we establish a first step toward the development of a novel, cost-effective, compact, fast, and non-destructive approach to probe non-uniform strain fields in semiconductor materials. To this aim, we propose to exploit the bulk photovoltage effect, which occurs in optically excited samples featuring a lattice strain gradient.

Typical experiments that exploit the bulk-photovoltaic effect can produce a map of a $20 \times 20\,\mathrm{cm}^2$ sample in less than 10 h, more than 50% less than the time required by a typical Raman setup. More importantly, such a measurement requires just a focused laser beam to locally excite the sample and the evaporation of two rim contacts to acquire the induced voltage as a function of the spot position, i.e., a very compact and cheap setup in comparison with the above-mentioned approaches.

The basic idea is to correlate the local mechanical deformation to the induced valence and conduction band edge energy shifts. When a laser beam is focused on the sample surface, the strain-induced variation in the band edge profiles drifts the excited electron–hole pairs. Since the hole and electron response to these drifts is different, a charge imbalance is obtained. This effect can be detected measuring the voltage difference between two rim contacts, placed at the boundary of the semiconductor sample. Scanning the sample surface with the laser spot, a map of the voltage variation can be acquired and, supported by finite element simulations, quantitatively correlated to the strain profile by means of a fitting procedure performed to calibrate the predicted voltages against the measured ones. The experimental setup here envisaged is identical to the one used to perform lateral-photovoltage-scanning (LPS) measurements.[26]

This technique was originally developed in the late 1990s to image, exploiting the bulk photovoltaic effect, the background doping striations typically present in bulk semiconductor crystals grown by the Czochralsky or the floating zone method, with a spatial resolution whose typically value is of the order of $100\,\mu$m.[27] The local resolution strongly improves in samples with high doping concentration since they feature reduced excess carrier lifetimes or more generally in samples featuring low mobility and/or carrier lifetime values. In general, the bulk photovoltaic effect is associated with the spatial inhomogeneity of the doping concentration, as theoretically addressed for the first time by Tauc.[28] Following the same line of reasoning proposed by Tauc, one can get easily convinced that any physical effect, which locally modifies the band edge profile of a bulk semiconductor, can produce a photovoltage signal. This fact suggests that a setup leveraging on the bulk-photovoltaic effect has a spatial resolution appropriate to map the strain field featured by SiN/Si microstructures.

RESULT AND DISCUSSION

As a first step to corroborate the viability of the LPS setup as a fast and cost-effective approach for the measurement of strain inhomogeneity in semiconductor samples, in this work, we numerically assess the photovoltage signal obtained from non-uniformly strained silicon samples.

More precisely, we simulate the spatial dependent photovoltage acquired scanning the (001) surface of moderately doped silicon wafers, featuring an array of silicon nitride (SiN) stressor stripes deposited on the top surface to induce a periodic distortion in the underlying lattice. Based on the spatial resolution of the LPS method and its sensitivity,[27] this system is expected to feature a detectable strain gradient, which at the same time can also be benchmarked with lattice deformation data obtained by means of typical micro-Raman experiments, similar to those reported in Refs. 10, 29, and 30.

Moreover, it is worth noticing that the material platform here investigated as a case study is of great applicative interest in the field of silicon photonics because the controlled lattice deformations induced in the Si material by the SiN stressor stripes reduce the lattice symmetry, thus allowing for second order non-linearities. Similarly, robust linear electro-optic effects, absent in centrosymmetric lattices, can be obtained.[11]

Furthermore, as recently reviewed in Ref. 31, silicon nitride waveguide technology opens new horizons for the development of a complementary platform for the silicon on insulator (SOI) photonics. With the availability of low loss waveguides adaptable to both linear and non-linear optical functions, this will expand the applications of optical signal processing, reducing the cost and size of electronic solutions.

We have studied two systems: an n-type Si wafer (n-sample) and a p-type one (p-sample), both featuring a dopant concentration of $5 \times 10^{16}\,\mathrm{cm}^{-3}$. Aftere evaluating the lattice deformation by means of 2D finite element mechanical simulations, we calculate its spatially resolved impact on the band structure. These data are subsequently used to simulate the steady-state 3D excess carrier spatial distribution produced when a well focused laser beam excites the sample from the top surface. Finally, the obtained carrier distribution allowed us to estimate as a function of the pump spot position $V_{ph}(x)$, defined as the variation of the voltage at right rim contact with respect to the equilibrium condition. Simulated samples, sketched in Fig. 1(a), consist of an infinitely wide slab of doped silicon with two rim contacts, parallel to the [010] crystallographic axis (the y direction), placed at a distance of 3 mm. The surface region between the contacts features a periodic array (five repetitions) of infinitely long compressively strained SiN stripes with vertical (the z direction) and transverse (the x direction) lengths of 500 nm and $40\,\mu$m, respectively. We set the distance between the two centers of adjacent stripes at $130\,\mu$m. We assume that the SiN layer deposited on the Si wafer to fabricate the stripes features an initial compressive stress whose value has been ranged in the 0–5 GPa interval. This stress is partially relaxed after the selective etching performed to fabricate the stripes. Indeed, after this process step, the SiN material is free to relax along the transverse direction of the stripe, while the longitudinal one remains blocked. As a result, the stripes induce a non-uniform strain field in the underlying Si lattice. We used a finite element approach, as implemented in the solid mechanics module of the COMSOL Multiphysics platform, to evaluate in the framework of macroscopic elasticity theory all the components of the spatially resolved strain tensor. The tensor trace, calculated at room temperature in the zy-plane for an initial stress of 4 GPa, is shown in the color map of Fig. 1.

Published under an exclusive license by AIP Publishing

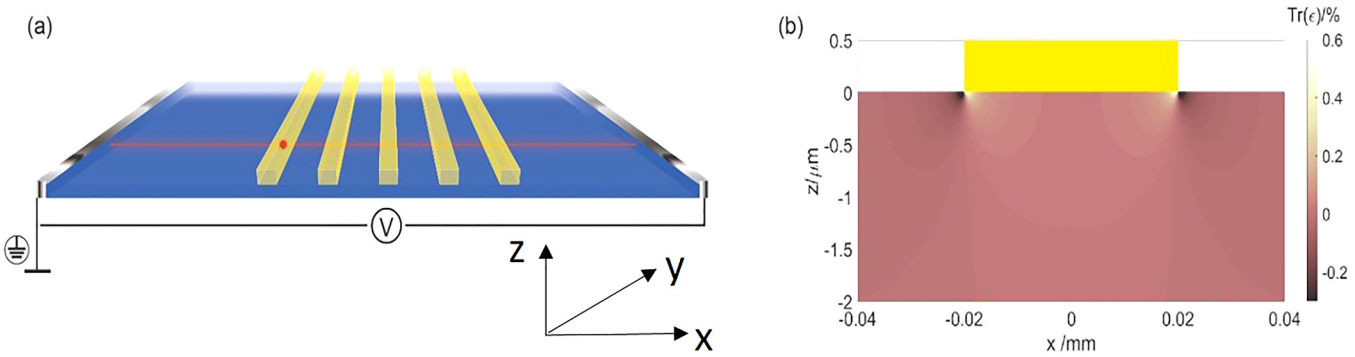


FIG. 1. (a) Sketch of the investigated samples with the adopted reference system. (b) Color map of the tensor trace in the stripe transverse plane *xz* in the lattice region under a stripe centered at $x = 0$ (the stripe vertical thickness is not in scale).

This figure indicates the presence of a modest tensile deformation, embraced by two more robust compressive lobes, located below the stripe boundaries. We estimate that the strain field along the vertical direction is almost extinguished for $z \geq 3\,\mu$m. In the top panels of Fig. 2, we report the *xx*, *zz*, and *xz* components of the strain tensor, evaluated along the x direction at 50 nm below the SiN/Si interface. The remaining components of ε_{ij} vanish due to the fact that the stripes cannot relax along the y direction. Notice that, in agreement with the system spatial symmetry, the ε_{xx} and ε_{zz} strain components are symmetric with respect to the *yz* plane passing through the stripe center, while the ε_{xz} one is antisymmetric.[32]

Also from Fig. 2, it is apparent that the deformation in the Si lattice is quite uniform and modest, except for large strain gradients that are present in small neighbors of about $0.5\,\mu$m centered at the stripe edges; here, peak values of the strain components are of the order of 1%. To evaluate the impact of this complex strain geometry on the excess carrier distribution, we have preliminary calculated the strain-induced band edge shifts in the *zx* plane using the deformation potential theory. To this aim, for the valence levels, we rely on the Bir–Pikus 6×6 Hamiltonian, adopting for the deformation potentials the literature values listed in Ref. 33. As shown in the first panel of Fig. 1, the nonvanishing strain components are only ϵ_{xx}, ϵ_{zz}, ϵ_{xz}. This allows us to simplify the Bir–Pikus Hamiltonian finding, three analytical expressions for heavy hole, light hole, and split-off bands that can be directly implemented into the COMSOL MultiPhysics approach, giving as an input for the semiconductor module the strain distribution obtained in the solid mechanics one. For what concerns the conduction band, the strain perturbation to the Δ band edges, located along the nonequivalent *x*, *y*, and *z* directions, has been calculated according to

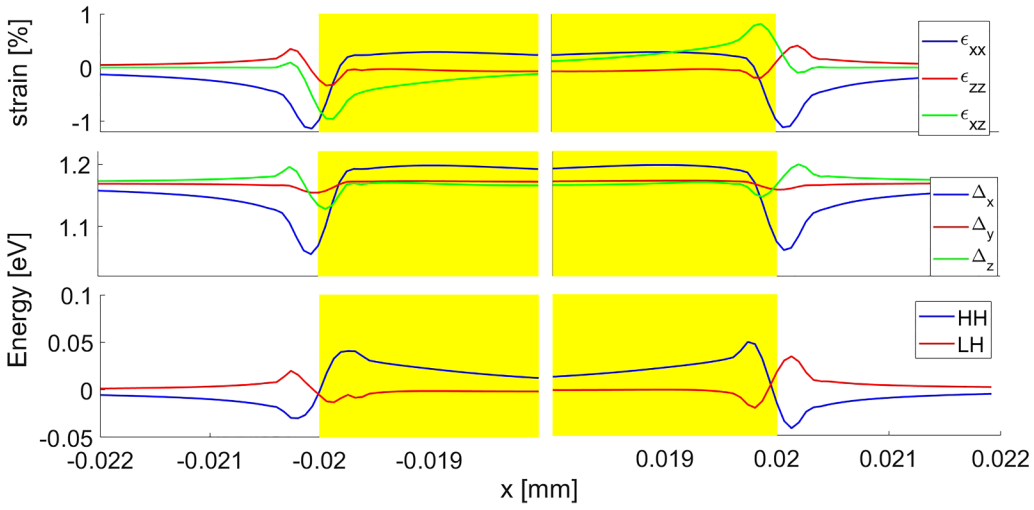


FIG. 2. Nonvanishing strain components (top), conduction Δ band edges energies (center), and heavy/light hole band edges (bottom), calculated as a function of x at $z = 50$ nm below the Si wafer surface. The yellow area indicates the stripe region centered at $x = 0$.

Published under an exclusive license by AIP Publishing

the analytical expression of Eq. (12) of Ref. 34, using the conduction deformation potentials there provided and directly implemented in COMSOL, as for the valence bands. The resulting band edge profiles, evaluated at 300 K for $z = 50$ nm, are shown as a function of x in the central and bottom panels of Fig. 2. We find valence and conduction band edge energy variations of the order of 70 and 150 meV, respectively. The bulk-photovoltaic effect at room temperature has been simulated relying on the Van Roosbroeck drift diffusion equations implemented, using the strain modified 2D band edge map, in the semiconductor module of the COMSOL Multiphysics platform. The electron–hole recombination dynamics has been calculated taking into account, besides the radiative channel, also the Auger and Schockley–Read–Hall mechanisms, implemented as detailed in Ref. 27. The adopted values for the Si and SiN material parameters present in the Van Roosbroeck equations have been taken from Ref. 35. We assume that at 300 K, hole carriers mainly populate the heavy hole (HH) band because of its much larger density of states with respect to the light hole (LH) one. For what instead concerns electrons, due to the strain-induced breaking of the Δ_6 degeneracy, we assume that the large majority of carriers occupies the (position dependent) Δ band edge featuring the lowest energy. At the adopted doping density, the equilibrium carrier electrons in the n-sample almost completely screen the drift forces associated with the bending of the conduction band edge shown in the center panels of Fig. 2. Therefore, the effective conduction band edge energy, obtained including in a self-consistent way the electrostatic contribution responsible for this screening effect, is constant along the x direction, and only the excess holes experience a drift force. This drift is associated with the effective valence band profile E_v shown in the top panel of Fig. 3 (blue curve), again obtained adding the Hartree potential to the HH bare profile reported in the bottom panel of Fig. 2. The opposite holds for the p-sample where the strain-induced drift force acts on the conduction carriers only since the valence band profile has been flattened by the spatial redistribution of the equilibrium holes. In this case, the effective conduction band edge profile E_c is shown in the bottom panel of Fig. 3.

Scanning the x direction with the pump laser spot ($\lambda = 685$ nm), we calculate $V_{ph}(x)$ as a function of the spot position centered at x. The quantity $V_{ph}(x)$ is evaluated as a potential difference between two ideal ohmic contacts located at the boundaries of the sample. The implementation of ideal ohmic contact in COMSOL assumes that there is thermo-dynamic equilibrium at the contacts. Moreover, the ohmic electrodes were located in an area of vanishing strain field of the stripes, in order not to alter the $V_{ph}(x)$ signal. In our simulations, the spot size was set at $\frac{1}{e^2} = 5\,\mu$m, and the power density at the external sample surface has been ranged between 12 and 6300 W/cm^2. The corresponding peak values for the excess carrier density are found in the 7.5×10^{13}–5.5×10^{16} cm^{-3} interval for both the n-doped and p-doped samples. Numerical calculations shown in Fig. 3 predict a robust photovoltage signal at room temperature. As expected, V_{ph}, with a spatial resolution of 10 nm, increases with the SiN initial stress. More precisely, in the explored range, the peak value of the photovoltage is a linear function of the SiN stress and typically increases at a rate of about 0.37×10^{-1} and 0.5 mV/GPa for the n- and p-samples, respectively. As for the spatial dependence of the signal, we notice that $V_{ph}(x)$ displays an oscillating behavior, whose spatial period matches the one of the stripe array. We have verified that, when the stripes do not feature an initial stress, $V_{ph}(x)$ identically vanishes. This fact guarantees that the optical non-uniformity of the Si surface, caused by the selective etching of the SiN material, does not introduce any artifact in the simulated photovoltage signal. To qualitatively interpret the behavior of $V_{ph}(x)$, we first discuss the n-sample. In this case,

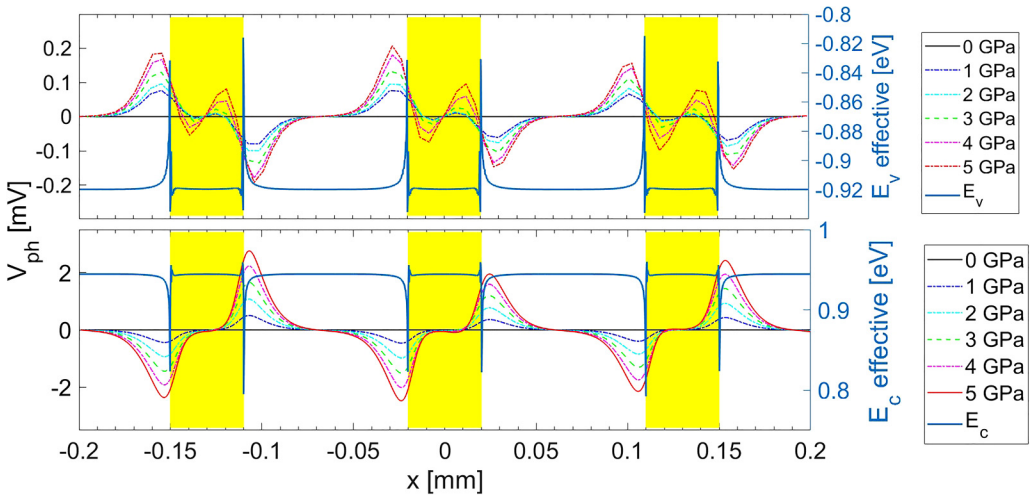


FIG. 3. Room temperature photovoltage V_{ph} (left vertical axis) as a function of the spot position x for the n- (top panel) and p-sample (bottom panel), calculated at different values of the initial SiN stress with a pump power density of 2×10^3 W/cm^2. The yellow area indicates the stripe regions. The blue solid curve refers to the right vertical scale and represents valence (top) and conduction (bottom) effective band edges.

Published under an exclusive license by AIP Publishing

the photovoltage features a well defined maximum (minimum) when the spot is focused in the external (internal) region of the stripe close to its left interface, located at x_L. The opposite holds when the laser is focused in the internal (external) region close to the right interface of the stripe at x_R since now, the $V_{ph}(x)$ signal features a maximum (minimum). We notice that in a neighbor centered in x_L and x_R, the strain-induced band edge variation in the effective valence profile acts as a confining potential for the holes (blue curve in the top panel of Fig. 3). As a consequence, exciting the sample at $x <\sim x_L$ ($x >\sim x_L$), we find that the spatial distribution of the excess hole features a sharp peak on its right (left) side, approximately centered at x_L (see the inset of Fig. 4).

In this way, the spatial distribution of excess holes results to be shifted rightward (leftward) with the respect to the excess carrier distribution in the conduction band. It follows that the pump induces an electrical dipole. When the spot is at $x <\sim x_L$ ($x >\sim x_L$), this dipole points toward the right (left) contact, resulting in a positive (negative) value for V_{ph}. The same line of reasoning allows us to interpret the behavior of V_{ph} observed when the spot is close to x_R. Also, the photovoltage signal V_{ph} induced in the p-sample can be qualitatively addressed relying on the same arguments. In this case, the excess holes move in an almost flat profile, while the motion of the excess electrons is influenced by the confining potential produced by the strain field close to the stripe boundaries (the bottom panel of Fig. 3). The resulting photo-induced dipole points toward the left and right contact when the spot is focused at $x <\sim x_L$ and at $x >\sim x_L$, respectively. The opposite holds when the pump spot is in a neighbor of x_R. We also notice that the signal in the internal stripe regions close to the boundaries is almost zero, and thus, the sign inversions observed in the corresponding region of the n-sample are absent. This behavior is to be attributed to intra-stripe cancellation effects, made possible by the larger mobility of the conduction carriers. As a final remark, we interpret the larger intensity of $V_{ph}(x)$ with respect to the n-doped system as mainly due to the higher resistivity of the p-Si material surrounding the excited region. We conclude our analysis briefly discussing the functional dependence of V_{ph} on the excitation density. In the explored range, the intensity of the photovoltage signal monotonically increases with the pump power. For instance, when the initial SiN stress is set at 4 GPa, upon increasing the laser power density between 12 and 6300 W/cm^2, the peak value of V_{ph} in the p- and n-samples covers the 0.2–4.3 and 0.01–0.8 mV range, respectively (see Fig. 4). In line with theoretical predictions reported in Ref. 28, we observe a sublinear increase of V_{ph}. Since the recombination dynamics is dominated, also in the high excitation regime, by the Shockley–Read–Hall (SRH) recombination mechanism, which is linear in the excess carrier density, this sublinear increase of V_{ph} has to be attributed to saturation effects associated with the excess carrier density. As a matter of fact, increasing the pump power, the larger density of minority carriers becomes more effective in screening the strain-induced band bending, thus suppressing in a more efficient way the driving forces responsible for the bulk photovoltage effect.

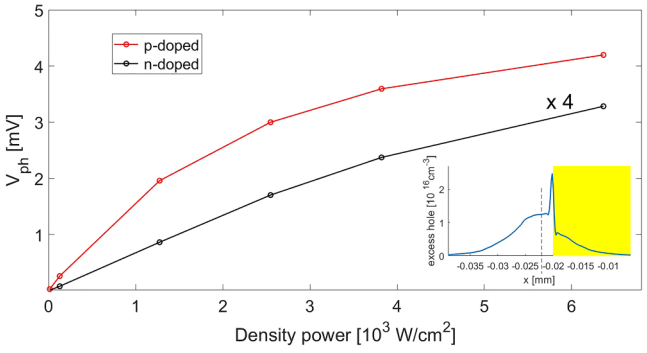


FIG. 4. RT peak intensity of the photovoltage signal V_{ph} in the n- (black) and p-sample (red) as a function of the pump power density for an initial SiN stress of 4 GP. The black curve has been rescaled. The inset shows the excess hole spatial distribution in the n-sample when the spot is focused at $x <\sim x_L$. The vertical dashed line and the yellow area indicate the spot center position and the stripe region, respectively.

CONCLUSION

In conclusion, we have shown that non-uniform strain fields in bulk semiconductor materials cause a photo-induced voltage at the sample boundary when a well focused laser beam is used to excite the system. To provide numerical evidence in this direction, we have analyzed as a case study p- and n-doped Si samples featuring an array of stressor stripes on the top surface. We find that even very modest strain fields, with peak values of the order of 0.1%, can originate photovoltage signals detectable at room temperature.

Although experimental validation of our numerical data is beyond the scope of the present paper, our results indicate that the photovoltage signal, in combination with numerical modeling, can be realistically used as a probe to quantitatively map the spatial dependence of strain fields in semiconductor lattices. This fact may have a noteworthy impact from an applicative perspective. We, therefore, believe that our findings may represent a first step toward the development of a cost-effective, compact, fast, and non-destructive characterization tool for strain imaging in semiconductor microstructures.

ACKNOWLEDGMENTS

The authors acknowledge Professor T. Schroeder for fruitful discussions, Dr. Thomas Koprucki for wise suggestions, and Chiara Fiore for graphical support.

AUTHOR DECLARATIONS

Conflict of Interest

The authors have no conflicts to disclose.

Ethics Approval

Ethics approval is not required.

Published under an exclusive license by AIP Publishing

DATA AVAILABILITY

The data that support the findings of this study are available from the corresponding author upon reasonable request.

REFERENCES

[1]Y. Sun, S. E. Thompson, and T. Nishida, J. Appl. Phys. **101**, 104503 (2007).
[2]M. Virgilio, C. L. Manganelli, G. Grosso, G. Pizzi, and G. Capellini, Phys. Rev. B **87**, 235313 (2013).
[3]A. Elbaz, D. Buca, N. von den Driesch, K. Pantzas, G. Patriarche, N. Zerounian, E. Herth, X. Checoury, S. Sauvage, I. Sagnes, A. Foti, R. Ossikovski, J.-M. Hartmann, F. Boeuf, Z. Ikonic, P. Boucaud, D. Grützmacher, and M. El Kurdi, Nat. Photonics **14**, 375 (2020).
[4]D. Stange, S. Wirths, R. Geiger, C. Schulte-Braucks, B. Marzban, N. von den Driesch, G. Mussler, T. Zabel, T. Stoica, J.-M. Hartmann, S. Mantl, Z. Ikonic, D. Grützmacher, H. Sigg, J. Witzens, and D. Buca, ACS Photonics **3**, 1279 (2016).
[5]V. Reboud, A. Gassenq, N. Pauc, J. Aubin, L. Milord, Q. M. Thai, M. Bertrand, K. Guilloy, D. Rouchon, J. Rothman, T. Zabel, F. Armand Pilon, H. Sigg, A. Chelnokov, J. M. Hartmann, and V. Calvo, Appl. Phys. Lett. **111**, 092101 (2017).
[6]M. El Kurdi, M. Prost, A. Ghrib, S. Sauvage, X. Checoury, G. Beaudoin, I. Sagnes, G. Picardi, R. Ossikovski, and P. Boucaud, ACS Photonics **3**, 443 (2016).
[7]C. L. Manganelli, M. Virgilio, M. Montanari, I. Zaitsev, N. Andriolli, S. Faralli, S. Tirelli, F. Dagnano, W. M. Klesse, and D. Spirito, Phys. Status Solidi A **218**, 2100293 (2021).
[8]K. Rim, J. L. Hoyt, and J. F. Gibbons, IEEE Trans. Electron Devices **47**, 1406 (2000).
[9]R. S. Jacobsen, K. N. Andersen, P. I. Borel, J. Fage-Pedersen, L. H. Frandsen, O. Hansen, M. Kristensen, A. V. Lavrinenko, G. Moulin, H. Ou, C. Peucheret, B. Zsigri, and A. Bjarklev, Nature **441**, 199 (2006).
[10]F. Bianco, K. Fedus, F. Enrichi, R. Pierobon, M. Cazzanelli, M. Ghulinyan, G. Pucker, and L. Pavesi, Semicond. Sci. Technol. **27**, 085009 (2012).
[11]C. L. Manganelli, P. Pintus, and C. Bonati, Opt. Express **23**, 28649 (2015).
[12]C. Castellan, A. Trenti, C. Vecchi, A. Marchesini, M. Mancinelli, M. Ghulinyan, G. Pucker, and L. Pavesi, Sci. Rep. **9**, 1088 (2019).
[13]M. Bouhassoune and A. Schindlmayr, Phys. Status Solidi C **7**, 460 (2010).
[14]J. G. Fiorenza, G. Braithwaite, C. W. Leitz, M. T. Currie, J. Yap, F. Singaporewala, V. K. Yang, T. A. Langdo, J. Carlin, M. Somerville, A. Lochtefeld, H. Badawi, and M. T. Bulsara, Semicond. Sci. Technol. **19**, L4 (2004).
[15]R. A. Minamisawa, M. J. Süess, R. Spolenak, J. Faist, C. David, J. Gobrecht, K. K. Bourdelle, and H. Sigg, Nat. Commun. **3**, 1096 (2012).
[16]G. Capellini, M. De Seta, P. Zaumseil, G. Kozlowski, and T. Schroeder, J. Appl. Phys. **111**, 073518 (2012).
[17]G. Capellini, G. Kozlowski, Y. Yamamoto, M. Lisker, C. Wenger, G. Niu, P. Zaumseil, B. Tillack, A. Ghrib, M. de Kersauson, M. El Kurdi, P. Boucaud, and T. Schroeder, J. Appl. Phys. **113**, 013513 (2013).
[18]M. Montanari, M. Virgilio, C. L. Manganelli, P. Zaumseil, M. H. Zoellner, Y. Hou, M. A. Schubert, L. Persichetti, L. Di Gaspare, M. De Seta, E. Vitiello, E. Bonera, F. Pezzoli, and G. Capellini, Phys. Rev. B **98**, 195310 (2018).
[19]E. Anastassakis and M. Cardona, *Semiconductors and Semimetals* (Elsevier, 1998), pp. 117–233.
[20]F. Cerdeira, C. J. Buchenauer, F. H. Pollak, and M. Cardona, Phys. Rev. B **5**, 580 (1972).
[21]M. J. Süess, R. A. Minamisawa, R. Geiger, K. K. Bourdelle, H. Sigg, and R. Spolenak, Nano Lett. **14**, 1249 (2014).
[22]O. Moutanabbir, M. Reiche, A. Hähnel, W. Erfurth, M. Motohashi, A. Tarun, N. Hayazawa, and S. Kawata, Appl. Phys. Lett. **96**, 233105 (2010).
[23]A. Gassenq, S. Tardif, K. Guilloy, I. Duchemin, N. Pauc, J. M. Hartmann, D. Rouchon, J. Widiez, Y. M. Niquet, L. Milord, T. Zabel, H. Sigg, J. Faist, A. Chelnokov, F. Rieutord, V. Reboud, and V. Calvo, J. Appl. Phys. **121**, 055702 (2017).
[24]S. Würzner, M. Herms, T. Kaden, H. Möller, and M. Wagner, Energies **10**, 414 (2017).
[25]A. Bashir, R. W. Millar, K. Gallacher, D. J. Paul, A. D. Darbal, R. Stroud, A. Ballabio, J. Frigerio, G. Isella, and I. MacLaren, J. Appl. Phys. **126**, 235701 (2019).
[26]S. Kayser, A. Lüdge, and K. Böttcher, IOP Conf. Ser.: Mater. Sci. Eng. **355**, 012019 (2018).
[27]S. Kayser, Ph.D. thesis, Brandeburg University of Technology, 2021.
[28]J. Tauc, Czech. Fiziceskij Z. **5**, 178 (1955).
[29]I. Olivares, T. Angelova, and P. Sanchis, Sci. Rep. **7**, 7241 (2017).
[30]M. Cazzanelli, F. Bianco, E. Borga, G. Pucker, M. Ghulinyan, E. Degoli, E. Luppi, V. Véniard, S. Ossicini, D. Modotto, S. Wabnitz, R. Pierobon, and L. Pavesi, Nat. Mater. **11**, 148 (2012).
[31]D. J. Blumenthal, R. Heideman, D. Geuzebroek, A. Leinse, and C. Roeloffzen, Proc. IEEE **106**(12), 2209 (2018).
[32]S. C. Jain, A. H. Harker, A. Atkinson, and K. Pinardi, J. Appl. Phys. **78**, 1630 (1995).
[33]C. G. Van de Walle, Phys. Rev. B **39**, 1871 (1989).
[34]C. G. Van de Walle and R. M. Martin, Phys. Rev. B **34**, 5621 (1986).
[35]S. Sze and K. N. Kwok, *Physics of Semiconductor Devices* (John Wiley & Sons, 1982).

Published under an exclusive license by AIP Publishing